PERFORMANCE EVALUATION OF THE BASE ISOLATION TECHNIQUE ON THE BLAST MITIGATION OF SPATIAL STRUCTURES

Kuppalli Krishne GOWDA KIRAN[1], Ehsan NOROOZINEJAD FARSANGI[2*]

[1] Assistant Professor, SJB Institute of Technology, Bangalore, Karnataka, India

[2] Assistant Professor, Faculty of Civil and Surveying Engineering, Graduate University of Advanced Technology, Kerman, Iran

Abstract

Unpredictable threat and danger may occur in a structural system due to blast loading. Long-span spatial structures are very practical and common in airport terminals, exhibition centers, stadiums, and other public buildings. For high-rise and multi-story structures, horizontal pressure plays a major role in the level of damage to a structure, whereas long-span structures may be influenced by both horizontal and vertical pressure. In the current study, the applicability of lead rubber bearing (LRB) has been evaluated on a low-rise, long-span structure. The analysis is carried out by using the MATLAB Simulink platform. The simulation results indicate that the base isolation system which is usually adopted for seismic control of structures can adequately reduce the structural responses under blast loadings.

Keywords: blast, base isolation, simulation, LRB, structural response

1. INTRODUCTION

Recently, the world has been facing severe threats due to terrorist activities, chemical explosions, and mining. Disasters may happen as a result of using

---

[*]Corresponding Author: Graduate University of Advanced Technology, Assistant Professor Ehsan Noroozinejad Farsangi, email: noroozinejad@kgut.ac.ir, Cell: +98-9134401569

heavy explosives materials. To safeguard structures against these manmade hazards, researchers are trying to prevent the damage by using cladding, dampers, and isolation methods [11,13,21,24,30]. Concrete structures such as beams, columns, and bridges that are exposed to blast loads have been analyzed by numerous researchers [14,34,42,45]. It is known that blast loading has high intensity and affects a localized part of the structure within milliseconds, whereas, seismic loads cause the damage at a smaller intensity but across the entire structure for several seconds or more [28].

Many researchers derived equations to calculate the blast load acting on the front wall, rear wall, and roof of a single degree of freedom (SDOF) system. The loads acting on the SDOF system are quantified in terms of pressure versus time [10,15,26,23,36,38]. The combination of pressure and impulse is known as the pressure impulse diagram (PI). It also plays a vital role in assessing the blast response in these structures. PI diagrams are used to assess the human response and to establish damage criteria for specific organs (e.g. eardrum, lungs, etc.) of the human body. The experimental method of finding out blast load response is an intricate phenomenon in which the analytical method is used. The procedure for plotting the PI diagram using the analytical approach is explained in the literature [9,12,25].

To analyze the response in seismic structures, the capacity spectrum method has been developed [29]. For irregular seismic inelastic structures, multi-mode pushover analysis is carried out by considering different load patterns, lateral forces, torques, and higher mode shapes [6,7,8,17]. The difference in the fundamental frequency of a structural system caused by the earthquake can be reduced by using the base isolation technique. The base isolation technique can be used in adjacent structures and fault flexible structures exposed to seismic force [4,20,19,22]. Base isolation with shape memory alloys is another alternative to reduce the response of multi-story buildings [16].

The dynamic behavior of a liquid storage tank exposed to seismic load has been considered as bi-directional. The liquid storage tank was connected to base isolation with LRB. The combinations of the liquid storage tank with base isolations resulted in increased damping and an improved isolation period of the structure [31]. To know the performance behavior of the isolation system under near-fault motions, interactions of the structural system were compared with and without the sliding base isolation [4,32,33].

Many researchers have analyzed the behavior of structural members exposed to blast load by considering only vertical pressure causing severe damage [24,27,35,37,39,40,41,44]. Few studies are available for the blast loadings on combinations of horizontal and vertical pressure on structures. In the present study, an attempt was made to analyze the damage caused by the blast load on a long span and low-rise structure by considering horizontal and vertical pressure.

It was found that the response was considerably reduced with the use of a base isolation system (LRB 100). The pressure impulse diagram, story drift ratio, lateral force, and inter-story displacement are the results of the present work.

2. LOW RISE AND LONG SPAN GRID STRUCTURE UNDER BLAST LOADING

Fig.1. represents the elevations of a low-rise long grid structure. It consists of 6 bays at 4.50m spacing, the height of the ground floor is 4.57m and the remaining floor has a height of 3.96m. Tables 1 and 2 represent the dynamic properties and blast load parameters of the structural system. The following are the assumptions made in the study:

−   Both blast load pressure and ground accelerations are considered.
−   The response is considered in both the X and Y directions.
−   Three mode shapes are considered.
−   The nonlinear dynamic response is considered.
−   The superstructure floors are assumed to be rigid.
−   During blast loading on the structure, no overturning and tilting occur when base isolations become active.
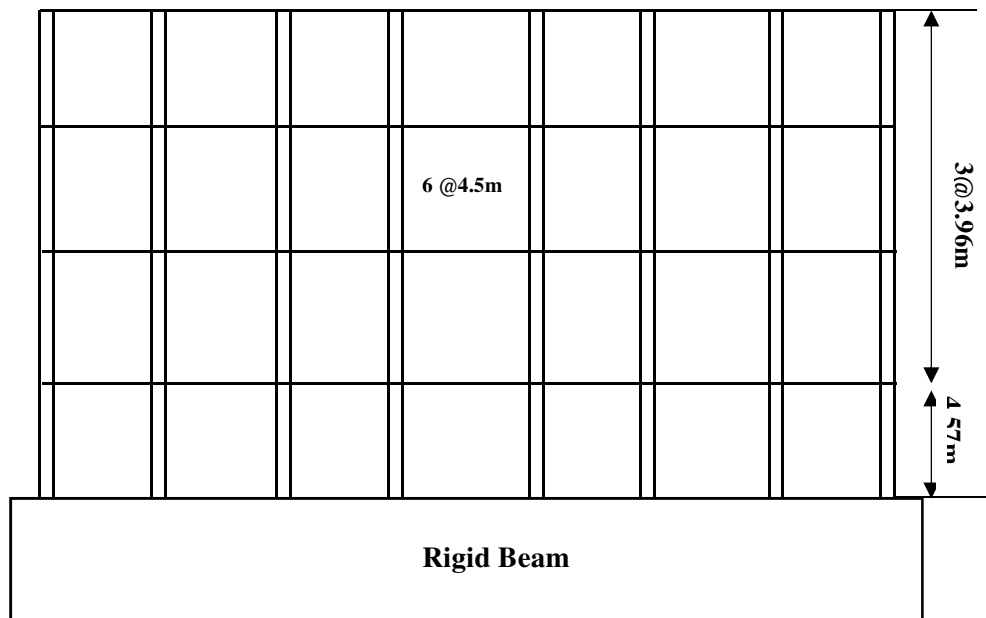

Fig. 1. Elevation of a low-rise and long-span grid structural system [18,43]

The following are the governing equations considered for a structural system under blast loading [3,4]

$$[M]\{\ddot{x}\} + [C]\{\dot{x}\} + [K]\{x\} = \{P(t)\} + \ddot{g} \tag{2.1}$$

Where M is the mass of the structure, C is the damping, K is the stiffness, P(t) is the pressure due to blast load, and $\ddot{g}$ is the ground accelerations, all in matrix format.

$$\{x(t)\} = Z_n \theta_n(t) \tag{2.2}$$

Where x(t) is the displacement, Zn is the time-dependent mode shape vector and θ_n is a time-dependent scalar vector.

$$(-\omega_n{}^2[M]Z_n + [K]Z_n)\theta_n(t) = 0 \tag{2.3}$$

Where ω_n is the natural frequency.

$$\phi_n = tan^{-1}\left[\frac{2\xi_n \frac{w}{w_n}}{1 - \frac{w}{w_n}^2}\right] \tag{2.4}$$

Where ϕ_n is the mode shape vector.

$$P = P^o\left(1 - {}^t/_{t_d}\right)e^{-\alpha t/t_d} \tag{2.5}$$

Where P is the pressure, Po is the peak overpressure, α is the decay constant, and td is the maximum time durations.

$$\frac{I}{A} = \text{Impulse per unit area} = \int_0^{t_d} p\, dt = P^o t_d\left[\frac{1}{\alpha} - \frac{1}{\alpha^2}(1 - e^{-\alpha})\right] \tag{2.6}$$

Table 1. Physical and Dynamic parameters of the structural system

No.	Parameter	Magnitude
1	Length	4.0m
2	Width	2.7m
3	Height	16.45m
4	Floor	4
5	Mass	11213kg
6	Stiffness	21860e3 N/m
7	Damping	5%

Table 2. Blast load parameters of a structural system

No.	Parameter	Magnitude
1	Range (R)	50.0 m
2	Scaled distance (Z)	3.73 m/kg1/3
3	Peak positive pressure (Pso)	74.3 kPa
4	Time of arrival (ta)	69.0msec
5	Wavelength (Lw)	12.2m
6	Negative phase duration (to)	52.2 msec
7	Positive impulse (is)	1025 kPamsec
8	Reflected pressure (Pr)	191.1 kPa
9	Reflected impulse (ir)	2338 kPamsec

3. BASE ISOLATIONS WITH THE LRB SYSTEM

Fig.2. represents the configurations for a lead rubber bearing (LRB 100), where 100 indicates the diameter of the LRB. Fig.3 represents the elevations of the low-rise, long-span structural system with LRB 100. It also shows the element point located on the plan of the structural system. Tables 3 and 4 represent the geometric and dynamic properties of the LRB 100 system.
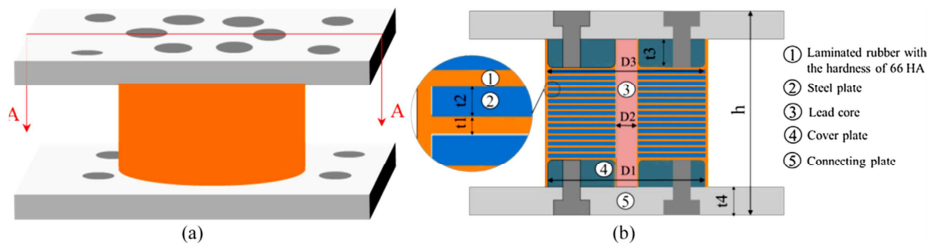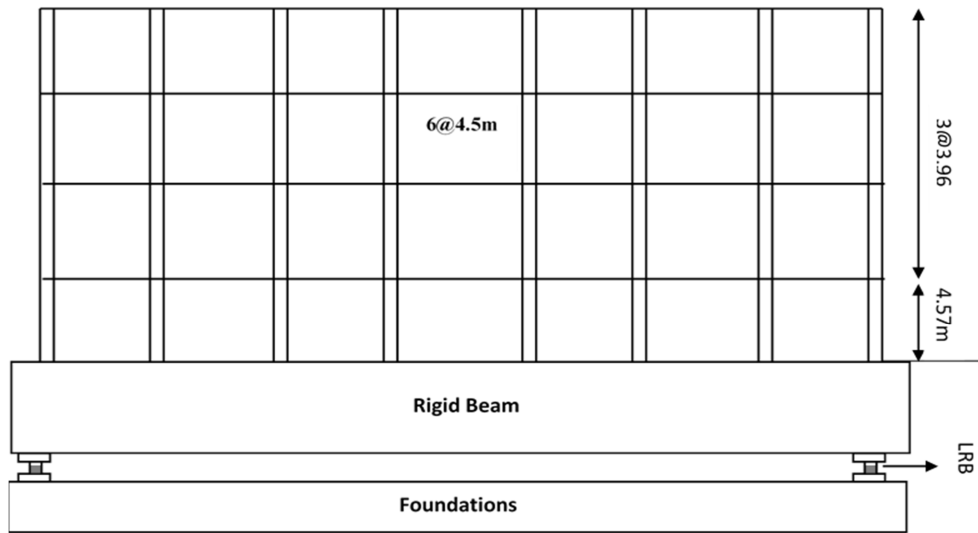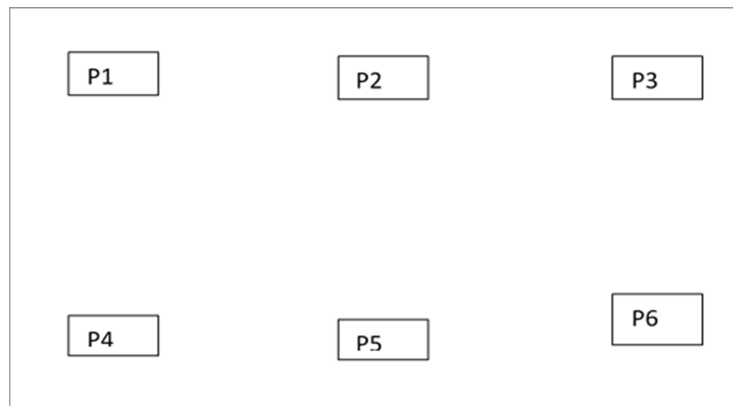

Fig. 2. Configurations of LRB 100: (a) 3D view, (b) A-A section view [43]

(a). Elevation

(b). Plan

Fig. 3. Elevation of a low-rise and long-span grid structural system with LRB 100 [42]

Table 3. Geometric Parameters of LRB 100

No.	Parameters	Value
1	Outer diameter of steel plate (D1)	100 mm
2	Diameter of lead core	14 mm
3	Thickness of single rubber (t1)	1.2 mm
4	Number of rubber layers	16
5	First shape coefficient (S1)	17.9
6	First shape coefficient (S2)	5.21
7	Thickness of the steel plate (t2)	2 mm
8	Diameter of the cover plate (D3)	10000
9	Thickness of the cover plate (t3)	15 mm
10	Thickness of connecting plate (t4)	20 mm
11	Height of LRB (h)	119.2 mm

Table 4. Dynamic properties of LRB 100

No.	Dynamic Properties	Magnitude
1	Stiffness (k)	29.26 kN/mm
2	Total yield force (Q)	8.21 kN
3	Mass	11290 kg
4	Pre-yield period	0.123 sec
5	Damping ratio (ξ)	0.02

The following equations are used for the LRB 100

$$K_h = \frac{Q_1 - Q_2}{X_1 - X_2} \tag{3.1}$$

$$Q_d = \frac{(Q_{d1} - Q_{d2})}{2} \tag{3.2}$$

$$K_d = \frac{\left(\frac{Q_1 - Q_{d1}}{X_1} + \frac{Q_2 - Q_{d2}}{X_2}\right)}{2} \tag{3.3}$$

$$h_{eq} = \frac{2\Delta W}{\pi K_h (X_1 - X_2)^2} \tag{3.4}$$

$$K_v = \frac{P_2 - P_1}{Y_2 - Y_1} \tag{3.5}$$

Where K_h is the equivalent shear stiffness, Q_d is the yield force, K_d is the post yielding stiffness, h_{eq} is the equivalent damping ratio, X_1 and X_2 are the maximum and minimum values of the shear displacement, respectively. Q_{d1} and Q_{d2} are the positive and negative shear force and shear displacement, respectively.

4.   MULTI-MODE ADAPTIVE PUSHOVER ANALYSIS

Structural responses of the blast load structure are calculated by using the following equations [1]:

$$f_n = \alpha_n m \emptyset S_a(T_n, \varsigma_n) \tag{4.1}$$

Where f_n = load vector; $\emptyset$ = mode shape at nth mode; and S_a = spectral pseudo acceleration as a function of the vibration period T_n; ς_n = damping ratio at nth mode; α_n = effective modal participating mass ratio

$$\alpha_n = \frac{M_n{}^*}{M^*} \tag{4.2}$$

Where $M_n{}^*$ and M^* = effective modal mass of the nth mode and the blast mass of the structure, respectively

$$M_n{}^* = \frac{(\emptyset^T{}_n mi)^2}{\emptyset^T{}_n mi} \tag{4.3}$$

$$M_n{}^* = \sum_{j=1}^{N} m_j \tag{4.4}$$

In which m_j = blast mass of jth floor

5. RESULTS AND DISCUSSIONS

The four-story, long-span, blast load structure has six nodal points being P_1, P_2, P_3, P_4, P_5, and P_6 in the study. The responses are calculated by using multi-mode adaptive pushover analysis with maximum mode. The analysis is carried out using MATLAB Simulink. The energy released during blast load in terms of the pressure is used in the analysis, with both horizontal and vertical pressure and Impulse considered. The load acting on the structural system is initially at the maximum and gradually reduces. The two maximum pressures occurring in the structural system are reflected pressure and incident pressure. Impulse is the product of time and pressure. The response is calculated by considering all three modes with responses being displacement, velocity, accelerations, story drift ratio, inter-story displacement, non-dimensional pressure, energy, rate of energy, pressure time with different damping, stiffness ratio, pressure impulse curve, and peak accelerations, peak velocity, and peak displacement at 6 element points along the Y-axis.
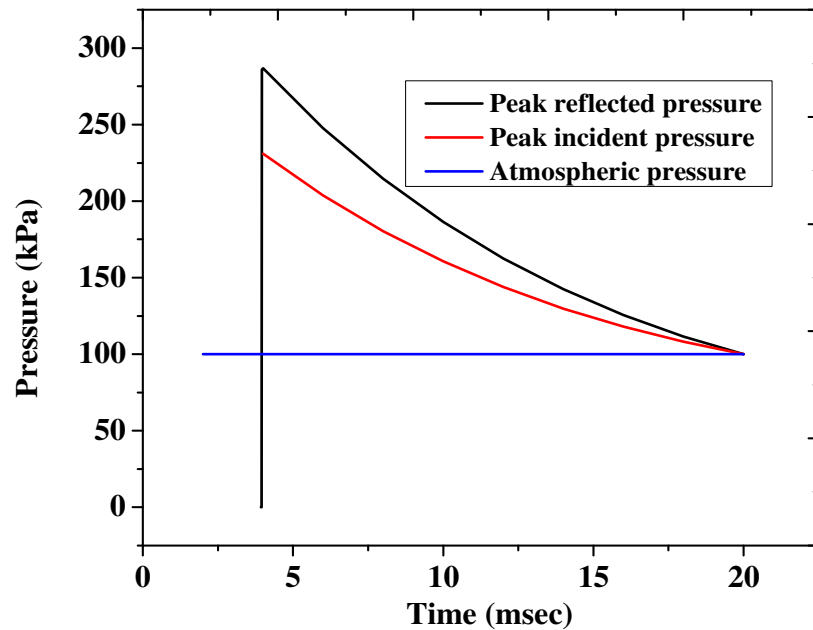

(a). Pressure time curve
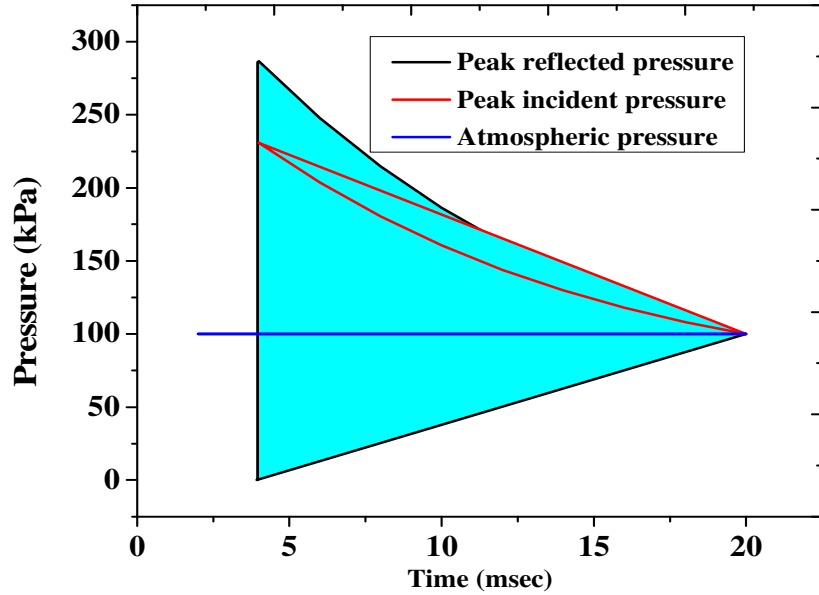
(b). Impulse time curve

Fig. 4. Blast loading time history curve

The pressure-time curve shown in Fig.4. (a) in which peak reflected pressure and incident pressure occur at 290kPa and 235kPa, at 4.5 msec. Fig.4. (b) shows that the impulse curve is the input parameter of the structural system exposed to the blast load. Fig.5. (a) shows that by using LRB 100, the reductions to maximum accelerations occurring on the second floor in the order of 0.33 m/msec^2 to 0.18 m/msec2, the third floor in the order of 0.23 m/msec^2 to 0.11 m/msec^2, and the third floor in the order of 0.22 m/msec^2 to 0.14 m/msec^2 are the values of the corresponding mode shapes 1,2, and 3. The minimum accelerations occurring on the fourth floor in the order of 0.25 m/msec^2 to 0.12 m/msec^2, the first floor in the order of 0.13 m/msec^2 to 0.4 m/msec^2, and first floor of 0.18 m/msec^2 to 0.1 m/msec^2 are the values of the corresponding mode shapes 1,2, and 3.
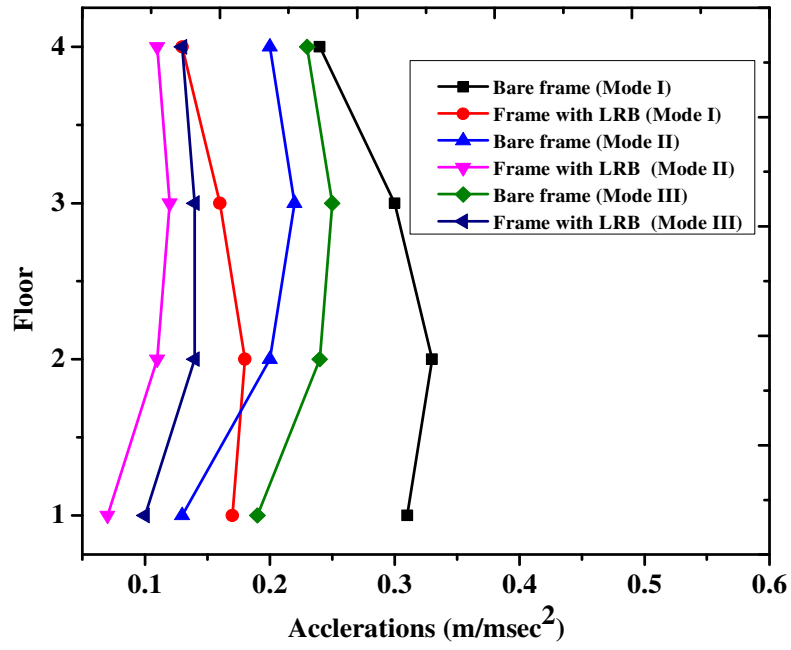
(a). Reductions of accelerations
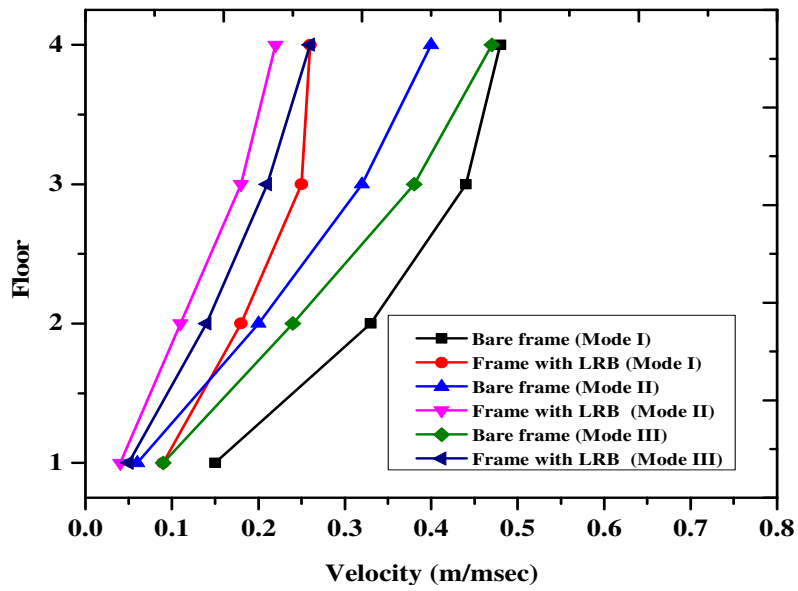
(b). Reductions of velocity
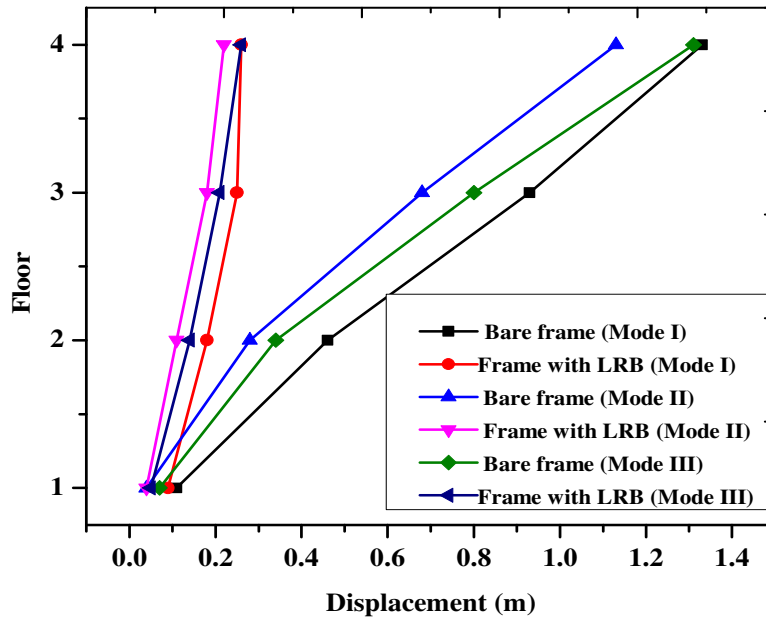
(c). Reductions of displacement

Fig. 5. Reduction of the structural responses

Fig.5. (b) shows that by using LRB 100, the reductions of maximum velocity occurring on the fourth floor in the order of 0.5 m/msec to 0.25 m/msec, the fourth floor in the order of 0.4 m/msec to 0.05 m/msec, and the fourth floor of 0.4 m/msec to 0.2 m/msec are the values of the corresponding mode shapes 1,2, and 3, and minimum velocity occurring on the first floor in the order of 0.15 m/msec to 0.10 m/msec, the first floor in the order of 0.05 m/msec to 0.04 m/msec, and the first floor in the order of 0.1 m/msec to 0.05 m/msec are the values of the corresponding mode shapes 1,2, and 3. Fig.5. (c) shows by using LRB 100, the reductions of maximum displacement occurring on the fourth floor in the order of 1.3 m to 0.2 m, the fourth floor in the order of 1.2 m to 0.2 m, and the fourth floor in the order of 1.2 m to 0.2 m are the values of the corresponding mode shapes 1,2, and 3, and the minimum displacement occurring on the first floor of 0.1 m to 0.09 m, the first floor of 0.06 m to 0.02 m, and first floor of 0.1 m to 0.02 m, are the values of the corresponding mode shapes 1,2, and 3.
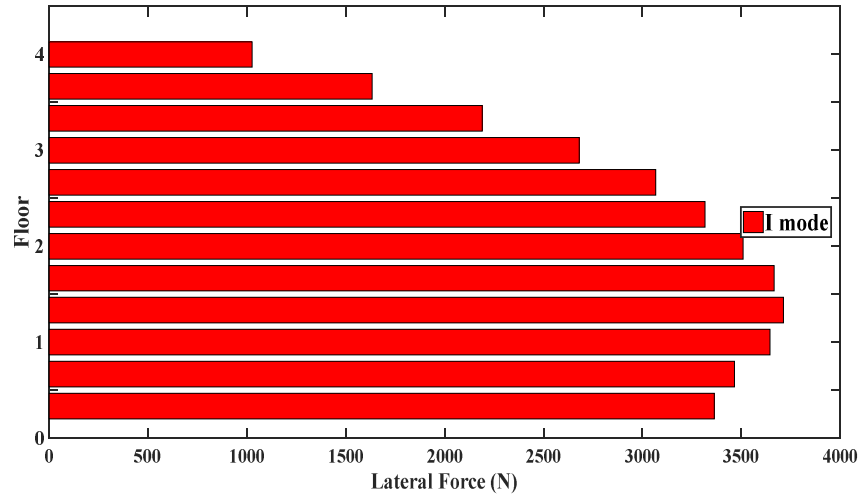
(a). First mode of lateral force
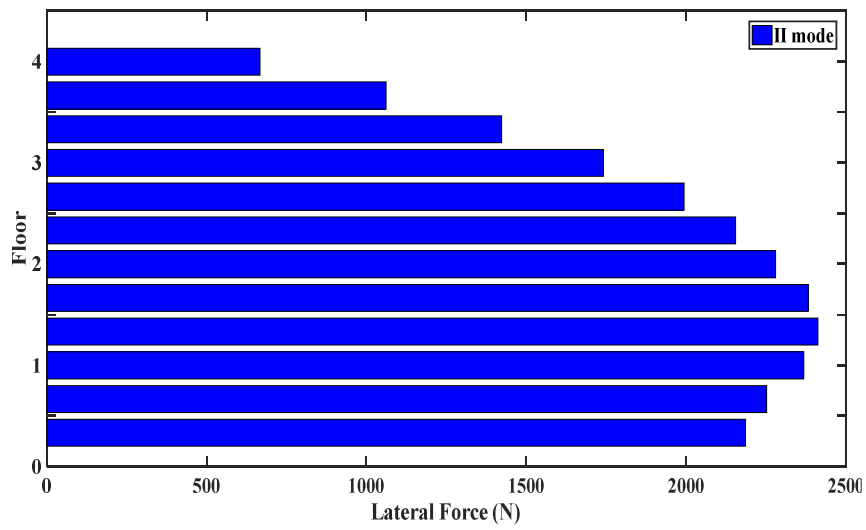
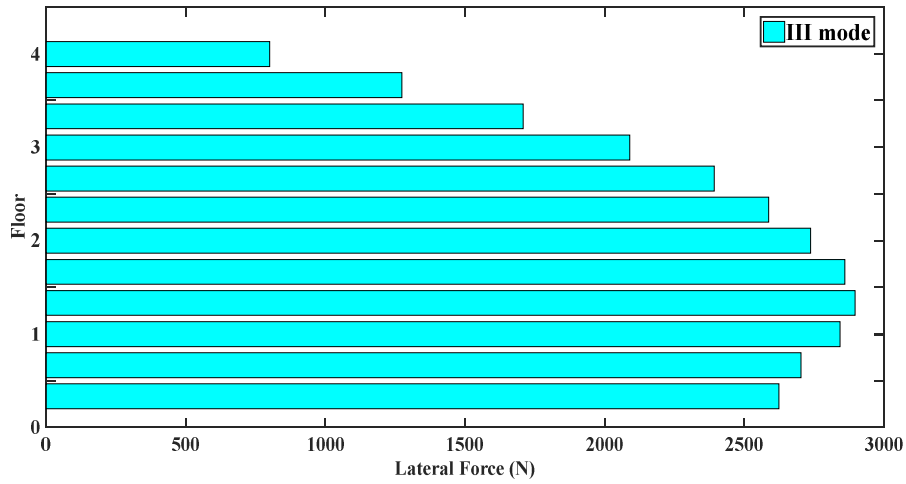(b). Second mode of lateral force

Fig. 6. Lateral forces acting on the structural system with different mode shapes

Fig.6. shows the lateral force of 3.8kN, 2.4kN, and 2.9kN at corresponding 1st, 2nd, and 3rd modes, respectively. Fig.7. shows the reductions of inter-story displacement of different modes by using LRB 100; the maximum inter-story displacement will be 0.65m for mode 1 and 0.38m for mode 2, and by using the LRB, the inter-story displacement is reduced to 0.4m for mode 1 and 0.38m for mode 2, the length of time of the inter-story displacement is 0.25msec.
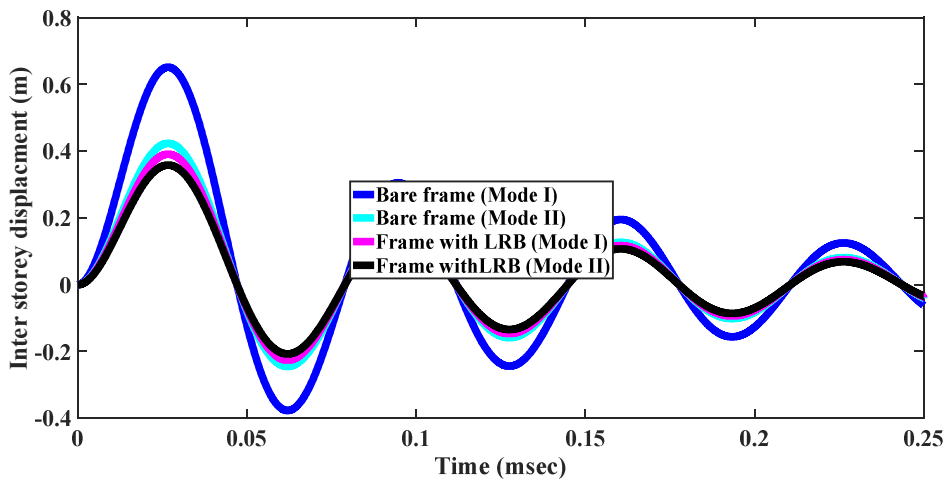
Fig. 7. Reduction of inter-story displacement with different mode shapes

Fig.8. shows the energy variations with time at different modes; the maximum energy occurs at 1st mode and minimum energy occurs at 3rd mode. Fig.9. shows the variations of the rate of energy (Impulse) and energy with different mode shapes. The maximum rate of energy occurs at 2% of damping and the minimum rate of energy occurs at 8% of damping. Fig.10. shows the variations of mode shape at different floors. The maximum mode shape occurs at the third mode and the minimum mode shape occurs at the second mode.
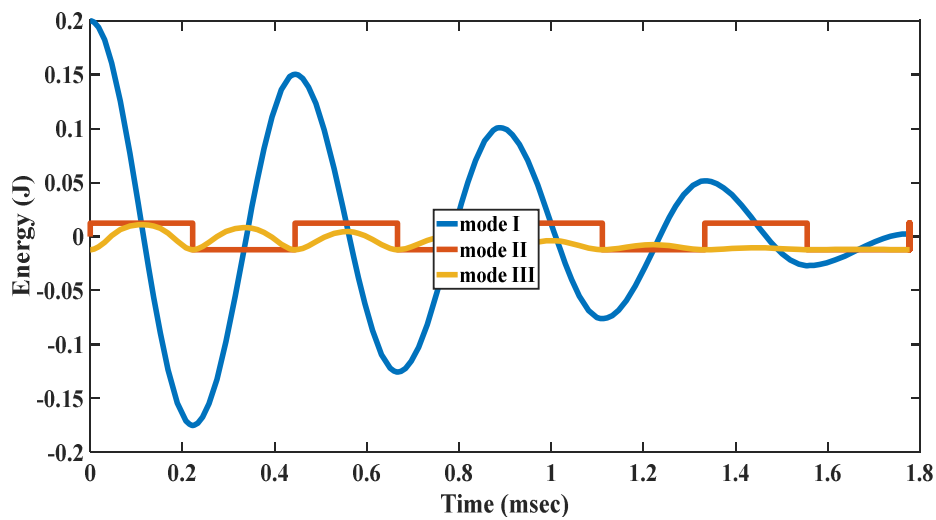

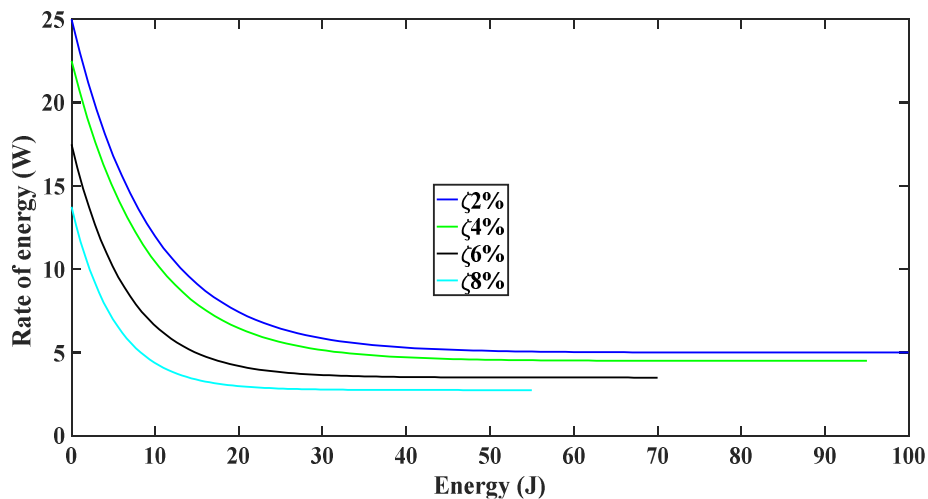Fig. 8. Variations of energy with time

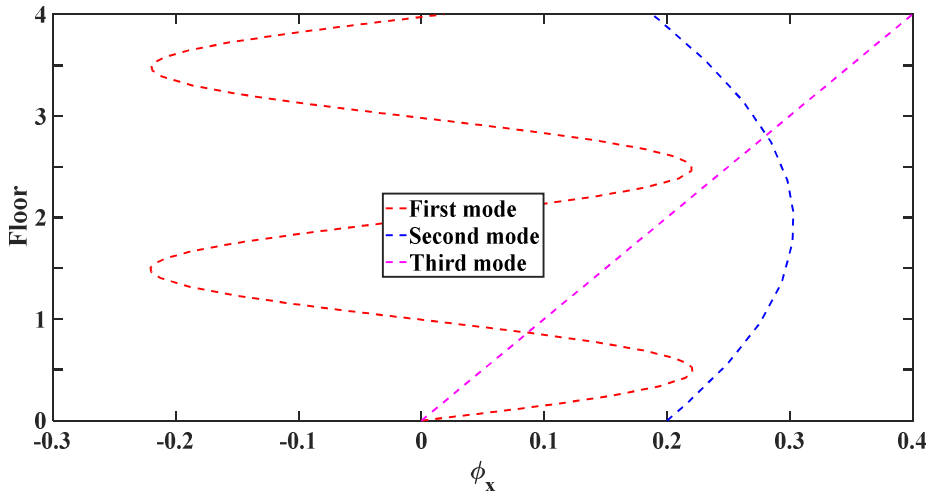Fig. 9. Rate of energy versus energy
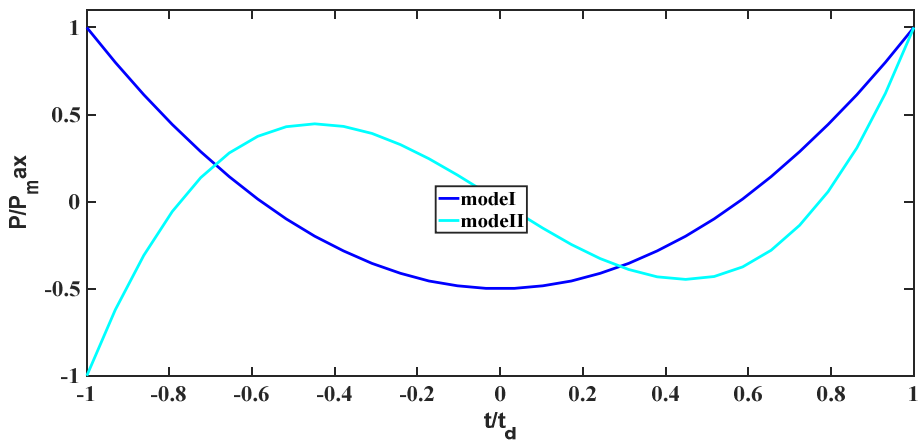
Fig. 10. Mode shape

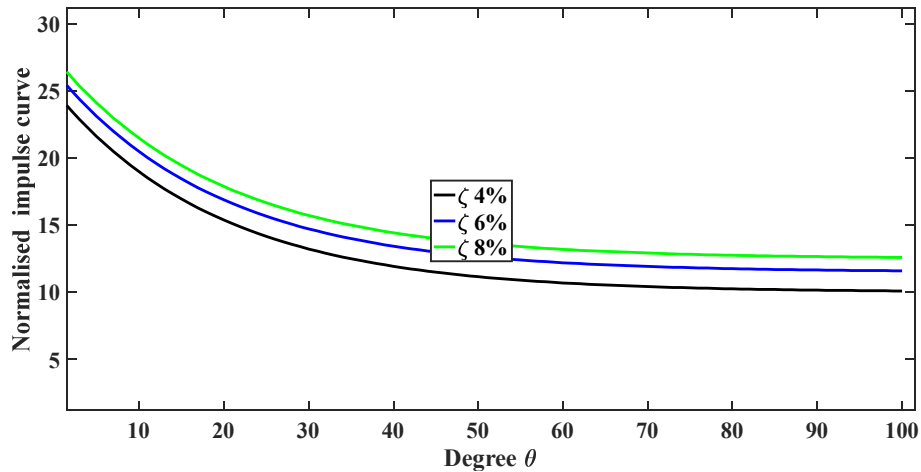Fig. 11. Non-dimensional pressure and time

Fig. 12. Normalized impulse curve and degree with different damping ratios

Fig.11. and Fig.12. show that the maximum non-dimensional pressure occurs at 1st mode and minimum non-dimensional pressure occurs at 2nd mode, maximum normalized impulse occurs at 8% damping, and there is a minimum 4% of damping. The non-dimensional pressure and time curve give the input parameter for calculating the response of the structural system and the performance of the structural system. The curve below the right corner will be the safe load for the structural system by using the LRB and the pressure increases from the bare frame to the frame with LRB will not affect damage to the structural system.
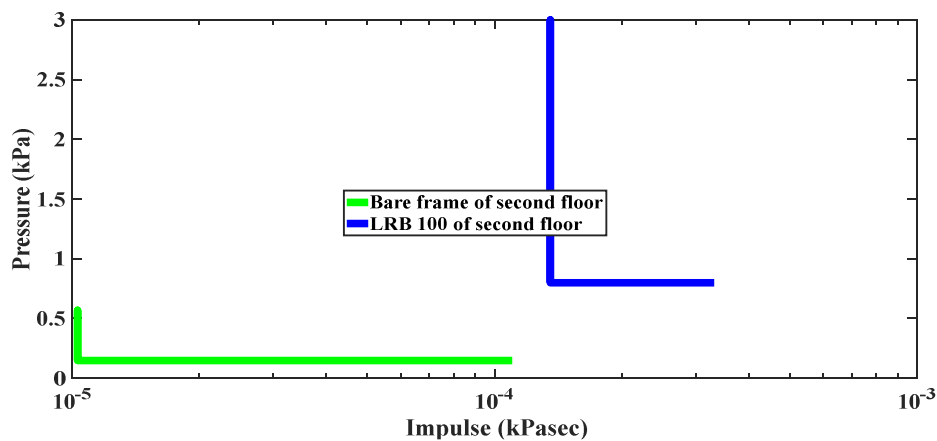

Fig. (a). Increase of pressure impulse curve by LRB 100 on the second floor
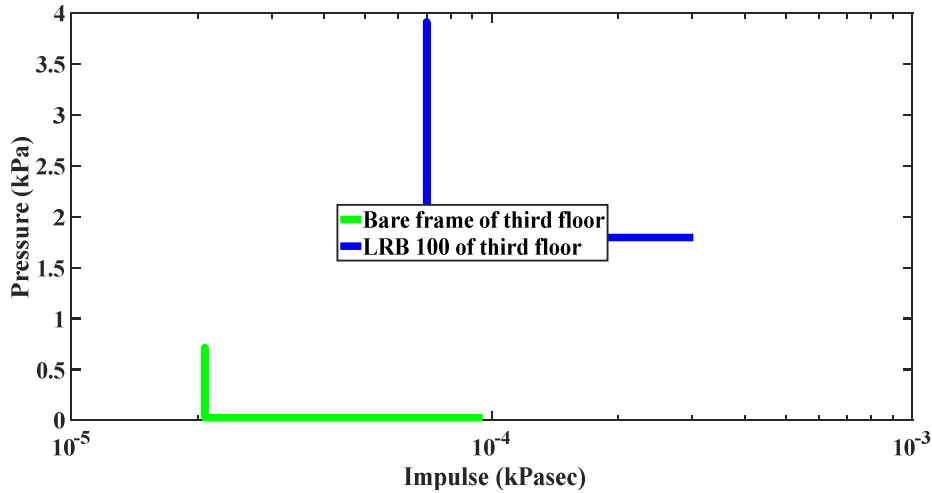
Fig. (b). Increase of pressure impulse curve by LRB 100 on the third floor

Fig. 13. Increase of pressure impulse curve by LRB 100 on the third floor

Fig.13. shows that by using the LRB 100 on the second floor, the pressure is increased from 0.5kPa to 1 kPa and the impulse rises from 0.1 Pasec to 1 Pasec, on the third floor, the pressure is increased from 0.1 kPa to 1.5 kPa and the impulse rises from 0.1 Pasec to 10 Pasec, the structure does not undergo failure. Fig.11. shows that mode III has the maximum pressure-time curve with damping of 8% and mode I has the minimum pressure-time curve with damping of 6%. The damping parameter plays a vital role in reducing the response to the structural system.
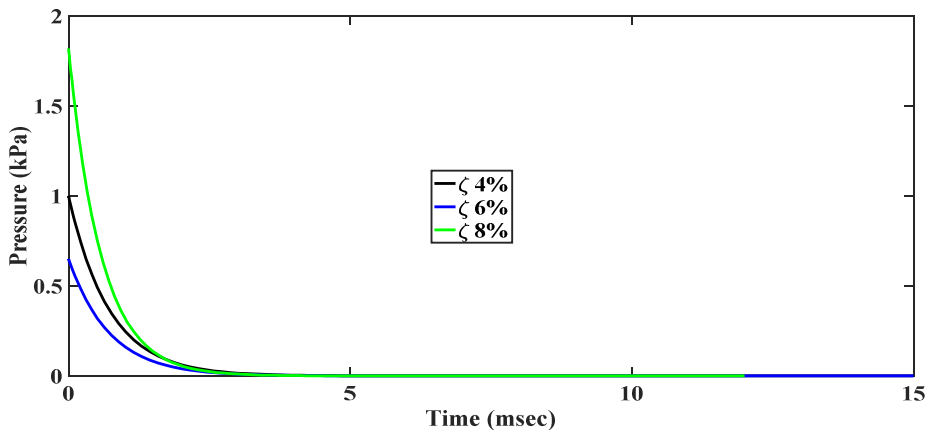
(a). First mode of pressure time curve
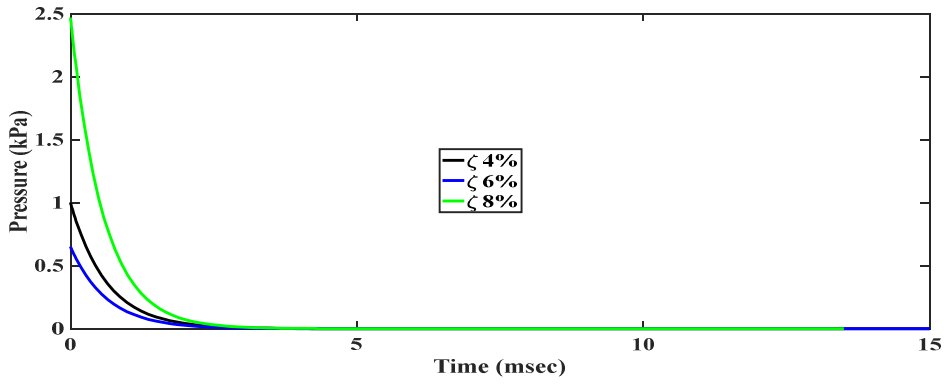
(b). Second mode of pressure time curve
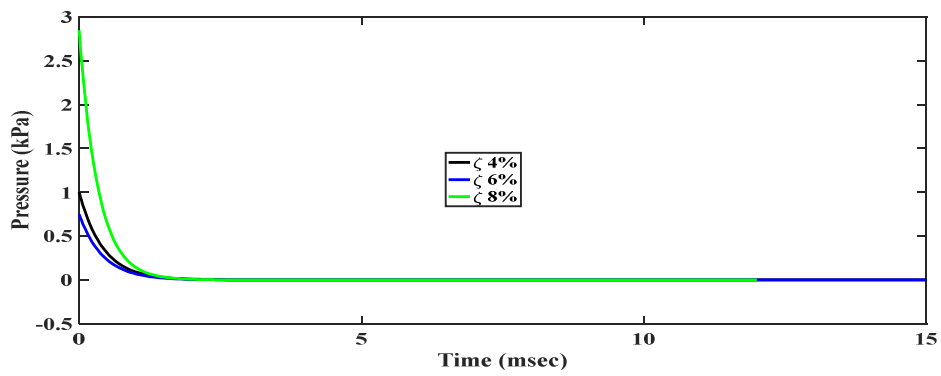
(c). Third mode of pressure time curve

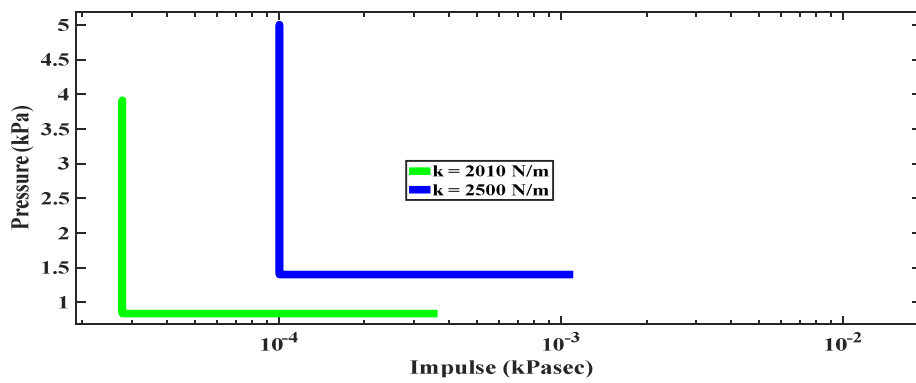Fig. 14. Pressure time curves with different mode

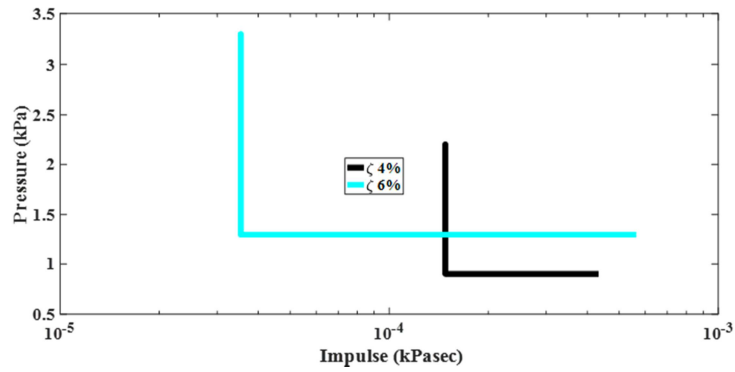Fig. 15. Pressure impulse curve with different damping ratio

Fig. 16. Pressure impulse curve with different stiffness

Fig.15. shows the pressure impulse curve with different damping ratios, the maximum pressure occurs at 6% damping. Fig.16. shows the pressure impulse curve with different stiffness, the maximum stiffness occurs at 2500 N/m. The pressure impulse curve is one of the main components of the structural system of the blast load.
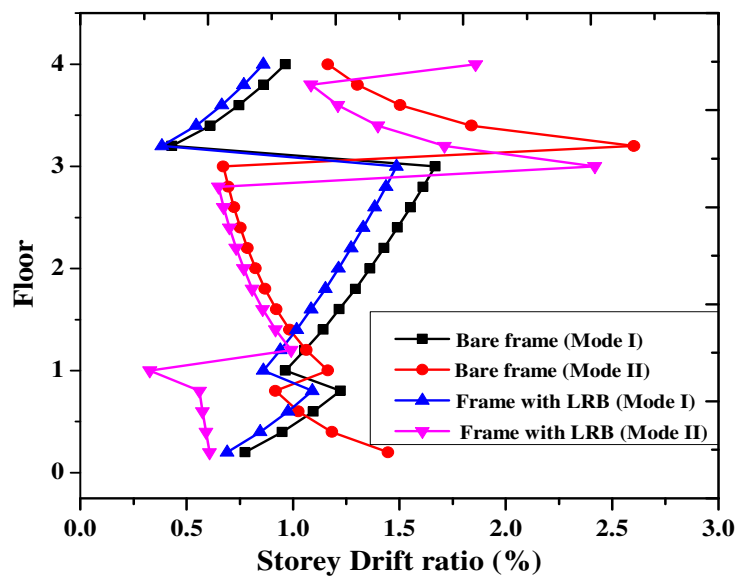

Fig. 17. The inter-story drift ratios obtained from single-mode and multi-mode pushover analyses

Fig.17 and Fig.18. show the reductions in inter-story drift ratio and mode shape resulting from the use of LRB 100. The maximum drift ratio occurs at mode II

on the third floor and the minimum story drift ratio is 3.5% for the third floor. The minimum drift ratio occurs at 0.5% for the first floor at Mode I. By using LRB, the 2nd mode plays a vital role in the reduction of the story drift ratio.
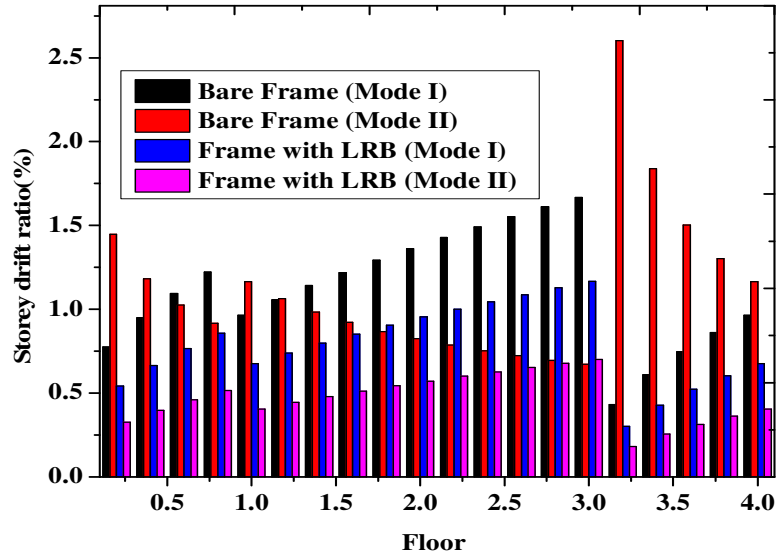

Fig. 18. Height distribution of the inter-story drift ratios obtained from single mode and multi-mode pushover analysis
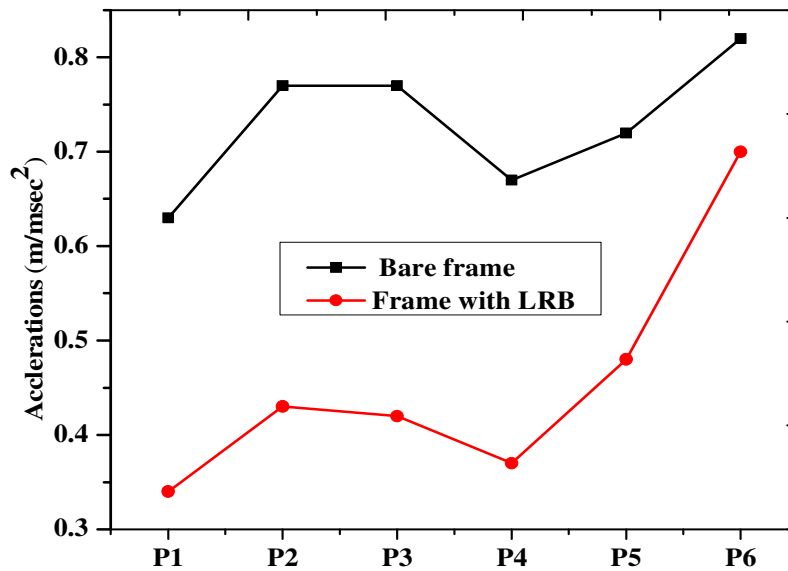

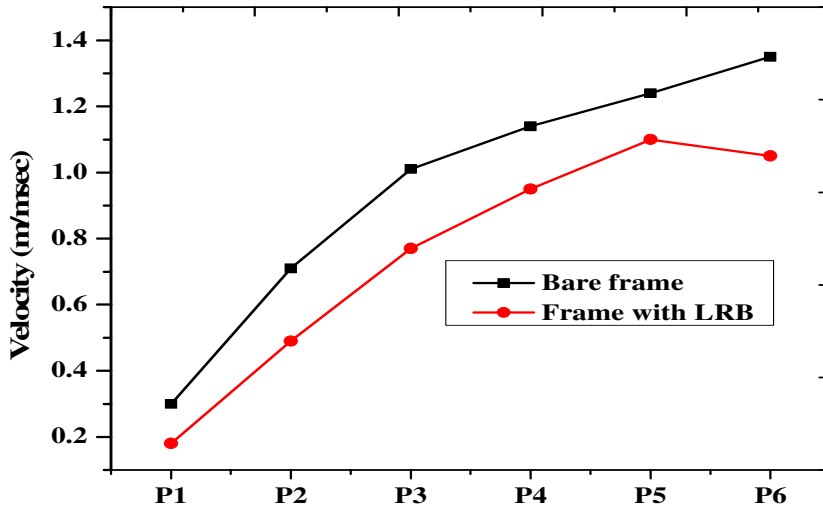Fig. 19. Vertical Peak accelerations

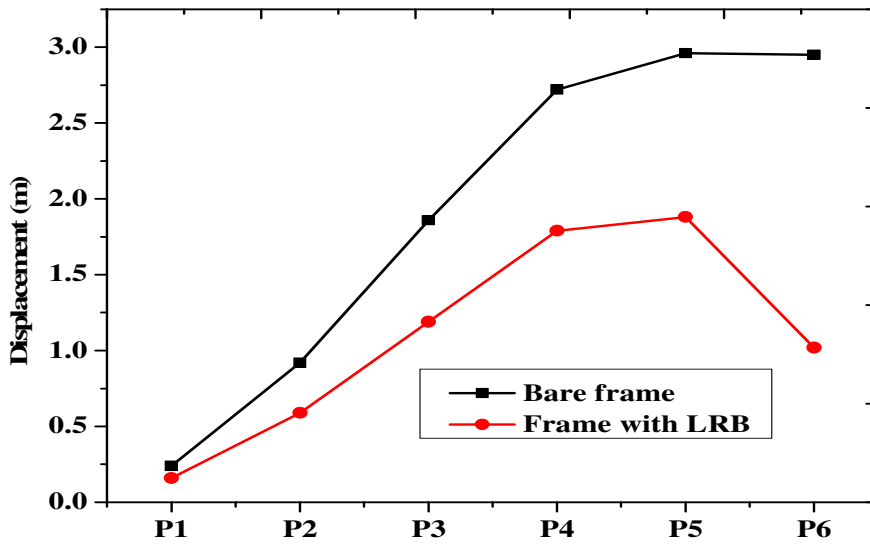Fig. 20. Vertical Peak velocity

Fig. 21. Vertical Peak displacement
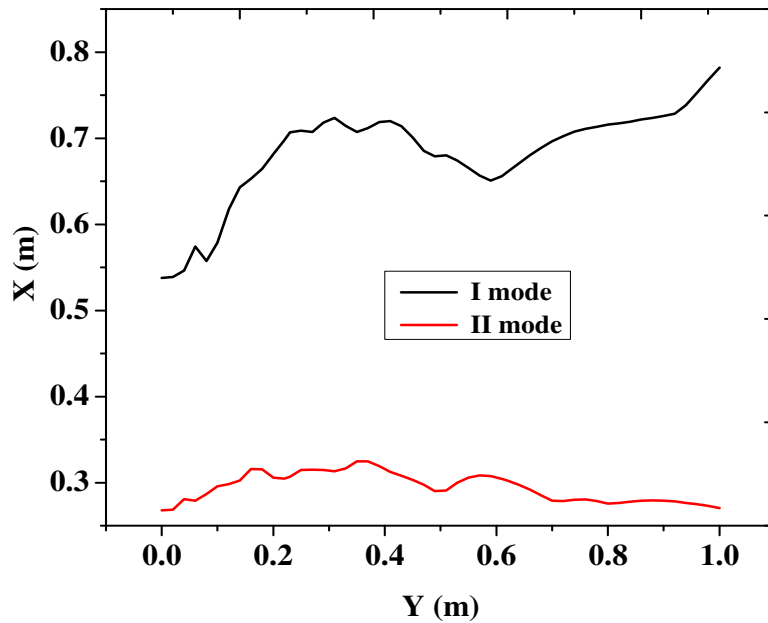
Fig. 22. Displacement track occurrence of isolated layer

Figs.19-21 show the reductions in peak vertical displacement by using LRB. The maximum acceleration occurs as 0.8 m/msec^2 and reduces to 0.7 m/msec^2, the maximum velocity occurs as 0.65 m/msec and reduces to 0.35m/msec, and the maximum displacement occurs at 1.4 m and reduces to 1 m at elements P1 and P6. Fig.22 shows the variations of the displacement along X and Y axes with two modes, the maximum displacement occurring along the X-axis is 0.8m and minimum displacement is at 0.55m, Y-axis maximum displacement occurs at 0.3m and minimum at 0.15m. The displacement occurring along the X-axis will be more compared to the Y-axis.

6. CONCLUSIONS

The current study investigates the long-span, low-rise blast load structure response and is calculated by using adaptative modal pushover analysis. The horizontal pressure, vertical pressure, and three mode shapes form the input parameters of the structural system. The six nodal element points, different damping and stiffness are the [output] parameters of the structural system. The main outcomes can be summarized as follows based on measured and calculated results:

− The multi-mode adaptive displacement-based pushover (MADP) analysis accurately estimates the blast load of RC moment-resisting frames.
− The different modes of inelastic mode shape are considered in MADP, also, different lateral force patterns are updated in each step of the analysis of a structural system.
− The increase of the blast load intensity on the long-span spatial structure with base isolation effectively increases the horizontal basic period, damping ratio, and significantly decreases the blast lateral forces.
− The vertical dynamic response of a base-isolated structure is very small, almost negligible. The horizontal acceleration response on a structural system with base isolation is significantly more, hence base isolation plays a vital role in the reduction of the response of a low-rise structure exposed to blast loads.
− The maximum response occurs in the 1st mode and by using LRB 100, the response is reduced by 49%.
− The maximum lateral force occurs in the 3rd mode.
− 20% reduction of inter-story displacement occurs in the 1st mode.
− The level of maximum floor story drift which occurs is high.
− The maximum response occurred at the P6 node.

REFERENCES

1. Amini, MA and Poursha, M 2018. Adaptive force-base multimode pushover analysis for seismic evaluation of midrise buildings, *Journal of Structural Engineering*, **144**, 1-12.
2. ASCE 2010. *Minimum design loads for buildings and other structures*. Reston, USA: American Society of Civil Engineers.
3. ASCE 2011. *Blast protection of buildings*. Reston USA: American Society of Civil Engineers.
4. Bhasker, RP and Jangid RS 2001. Performance of sliding systems under near-fault motions. *Nuclear Engineering and Design* **203**, 251-272.
5. Buckle, IG and Mayes, R L 1990. Seismic isolation: history, application and performance-a world overview. *Earthquake Spectra* **6**, 161-202.
6. Chopra, AK and Goel, RK 2002. A modal pushover analysis procedure for estimating seismic demands for buildings. *Earthquake Eng Struct Dyn* **31**, 561–82.
7. Chopra, AK and Goel, RK 2003. A modal pushover analysis procedure to estimate seismic demands for unsymmetrical-plan buildings: theory and preliminary evaluation. *Earthquake Engineering Research Center*.

8. Chopra, AK Goel, RK Chintanapakdee, C 2004. Evaluation of a modified MPA procedure assuming higher modes as elastic to estimate seismic demands. *Earthquake Spectra* **20**, 757–778.
9. CSA 2012. Design and assessment of buildings subjected to blast loads. Mississauga, Ontario: Canada.
10. Davis, C Sammarco, E Williamson, E 2017. *Bridge security design manual.* Washington, DC, USA.
11. Dusenberry, DO 2010. *Handbook of Blast-Resistant Design of Buildings*, John Wiley & Sons Inc.
12. FEMA 428, 2004. *Explosive blast. In: Risk management series.* Washington, USA.
13. FEMA, 2003. *Primer for design of commercial buildings to mitigate terrorist attacks*. Washington, USA.
14. FHWA, 2003. R*ecommendations for bridge and tunnel security, blue ribbon panel report*. Report No. FHWA-IF-03-036, Washington, DC, USA.
15. Gelfandetal, B Voskoboinikov, I Khomik, S 2004. Recording the position of a blastwave front in air. *Combust Explos Shock Waves* **40**, 734–6.
16. Ghodke, S and Jangid, RS 2016. Equivalent linear elastic viscous model of shape memory alloy for isolated structure. *Advances in Engineering Software*, **99**, 1-8.
17. Goel, RK and Chopra, AK 2004. Evaluation of modal and FEMA pushover analyses: SAC buildings. *Earthquake spectra* **20**, 225–54.
18. Jalilkhani, M Ghasemi, SH Danesh, M 2020. A multi-mode adaptive pushover analysis procedure for estimating the seismic demands of RC moment- resisting frames. *Engineering Structure*, **213**, 1-18.
19. Jangid, RS 2000. Optimum frictional elements in sliding isolation systems. Computer and Structures, **76**, 651-661.
20. Jangid, RS and Datta, TK 1995. Seismic behaviour of base isolated buildings – a state of the art review. *Journal of structures and Buildings*, **110**, 186-203.
21. Jones, N 2003. *Structural Impact*. Cambridge Press.
22. Kelly, JM and Konstantinidis, DA 2011. *Mechanics Of Rubber Bearings For Seismic And Vibration Isolation*.Wiley.
23. Kennedy, WD 1946. *Explosions and explosives in air.* Washington DC, USA.
24. Krauthammer, T 2005. *Modern Protective structures*. CRC Publications.
25. Krauthammer, T Astarlioglu, S Blasko, J Soh, TB Ng, PH 2008. Pressure–impulse diagrams for the behaviour assessment of structural components. *Int J Impact Eng*, **35**, 771–83.
26. Mays, GC and Smith, PD 2003. *Blast effects on Buildings*. Thomas Telford.

27. NCHRP 2005, Washington, DC, USA. *Blast-resistant highway bridges: design and detailing guidelines*. National Cooperative Highway Research Program.

28. Nourzadeh, D Humar, J Braimah, A 2017. Comparison of response of building structures to blast loading and seismic excitations, *Procedia Eng.* **210**, 320–325.

29. Paret, TF Sasaki, KK Eilbeck, DH Freeman, SA 1996. *Approximate inelastic procedures to identify failure mechanisms from higher mode effects*. In Proceedings of the eleventh world conference on earthquake engineering, 2.

30. Remennikov, AM 2002. Blast Resistant Consulting: A New Challenge for Structural Engineers. *Australian Journal of Structural Engineering* **4**, 121-134.

31. Shrimali, MK and Jangid, RS 2002. Non-linear seismic response of base-isolated liquid storage tanks to bi-directional excitation, *Nuclear Engineering and Design* **217**, 1-21.

32. Shrimali, MK and Jangid, RS 2002. Seismic response of liquid storage tanks isolated by sliding bearings. *Nuclear Engineering and Design* **24**, 909-921.

33. Shrimali, MK and Jangid, RS 2004. Seismic analysis of base-isolated liquid storage tanks. *Nuclear Engineering and Design* **275**, 59-75.

34. Smith, PJ 2013, New York, USA. *Terrorism in Asia: a persistent challenge sustained by ideological, physical, and criminal enablers*. In: *Handbook of Asian criminology*. Springer **147**–64.

35. TM-5-1300 1990, Washington DC, USA. *Design of structures to resist the effects of accidental explosions*, Technical Manual.

36. TM-5-855-1 1986, USA. *Fundamentals of protective design for conventional weapons*. Technical Manual.

37. US Department of Defense 2002, USA. *Design and analysis of hardened structures to conventional weapons effects*. UFC 3-340-01. Unified Facilities Criteria.

38. US Department of Defense 2008. *Structures to resist the effects of accidental explosions*. Report no. UFC 3-340-02. United Facilities Criteria.

39. US Department of Défense 2012, USA. *DoD minimum antiterrorism standards for buildings*. Report no. UFC 4-010-01.

40. US General Services Administration (GSA) 2003. *ISC security design criteria for new federal office buildings and major modernization projects*.

41. Williamson, EB et al. 2010. *Blast-resistant highway bridges: design and detailing guidelines*, USA National Cooperative Highway Research Program Rep. No. 645.

42. Williamson, EB Winget, DG 2005. Risk management and design of critical bridges for terrorist attacks. *J Bridge Eng*, **10**, 96–106.
43. Xu, W Du, D Wang, S Liu, W Li, W 2019. Shaking table tests on the multi-dimensional seismic response of long span grid structure with base isolation. *Engineering Structure* **201**, 1-16.
44. Zhang, C Gholipour G Mousavi AA 2019. Blast loads induced responses of RC structural members: State-of-the-art review *Composite* **195**, 1-24.
45. Zhang, F Wu, C Zhao, X-L Heidarpour, A Li, Z 2016. Experimental and numerical study of blast resistance of square CFDST columns with steel-fibre reinforced concrete. *Eng Struct* **149**, 50–63.